PCCP

PAPER

View Article Online
View Journal | View Issue

Cite this: *Phys. Chem. Chem. Phys.*, 2025, **27**, 9152

Ultrafast competition between CO release and spin crossover upon photoexcitation of a cyclopropenone-bipyridyl Fe^{II} complex†

Sebastian Megow, *[a] Annika Prax,[a] Tjorge Neumann,[b] Marc Lehr,[b] Anna J. McConnell *[bc] and Friedrich Temps *[a]

Received 2nd January 2025,
Accepted 7th April 2025

DOI: 10.1039/d5cp00019j

rsc.li/pccp

The photo-triggered release of carbon monoxide (CO) from a cyclopropenone-bipyridyl ligand and its iron(II) complex was investigated using a combination of stationary and ultrafast time-resolved spectroscopies. Upon continuous irradiation, the complex undergoes CO release and forms the corresponding acetylene photoproduct, albeit at *a* ∼ 3 times lower rate than the free cyclopropenone ligand, indicating a drastic reduction in quantum yield. We attribute this to the ultrafast dynamics revealed by femtosecond time-resolved electronic absorption spectroscopy, where photoexcitation of ligand-centered states of the complex is predominantly followed by energy-transfer, leading to spin-crossover of the Fe^{II} ion rather than CO release. This ultrafast response stands out as highly remarkable as it virtually outcompetes the photo-decarbonylation, which in the free ligand occurs in only ∼130 fs.

Introduction

The photo-initiated release of carbon monoxide (CO) from cyclic ketones has been a subject of ultrafast spectroscopic studies from the very beginnings of femtochemistry to the present.[1,2] For the decarbonylation and formation of the respective acetylenes from cyclopropenones, for example, time scales of <200 fs and quantum yields near unity have been reported.[3–5]

In a new development, McConnell and co-workers recently reported a promising new class of CO-releasing molecules, M-CPOnes, where **1** containing a cyclopropenone (CPOne) connected to a 2,2′-bipyridine functions as a ligand in a transition metal coordination complex (*e.g.*, Fe-CPOne, **Fe-1**, Fig. 1).[6] Using such scaffolds, varying the central metal ion and the second cyclopropenone substituent offers vast possibilities to access a broad range of M-CPOnes with attractive properties regarding stability, solubility, metal-ligand interactions and photochemical reactivity.[6] Indeed, varying the transition metal from Zn^{II} to Co^{II} and ultimately Fe^{II} led to a significant increase in the time required for complete decarbonylation upon irradiation with a 365 nm LED in NMR studies.[6] Furthermore, a colour change was observed upon photodecarbonylation of **Fe-1** to **Fe-2** (both diamagnetic low-spin Fe^{II} complexes) due to a hypsochromic shift of the MLCT band (Fig. 2B).

Here, we investigate how the coupling between cyclopropenone-bipyridyl ligands and the transition metal centre in **Fe-1** impacts the photodynamics. To this end, we apply femtosecond time-resolved electronic absorption spectroscopy (fs-TEAS) to shed light on both the mechanism of CO release leading from the free

[a] *Institute of Physical Chemistry, Christian-Albrechts-University Kiel, Olshausen-straße 40, 24098 Kiel, Germany. E-mail: megow@phc.uni-kiel.de, temps@phc.uni-kiel.de*
[b] *Otto Diels-Institute of Organic Chemistry, Christian-Albrechts-University Kiel, Olshausenstraße 40, 24098 Kiel, Germany*
[c] *Department Chemie-Biologie, University of Siegen, Adolf-Reichwein-Straße 2, 57068 Siegen, Germany. E-mail: anna.mcconnell@uni-siegen.de*

† Electronic supplementary information (ESI) available: DFT and TD-DFT calculations, additional stationary UV-vis spectroscopy results, additional fs time-resolved electronic absorption spectroscopy (fs-TEAS) results, syntheses of the sample compounds. See DOI: https://doi.org/10.1039/d5cp00019j

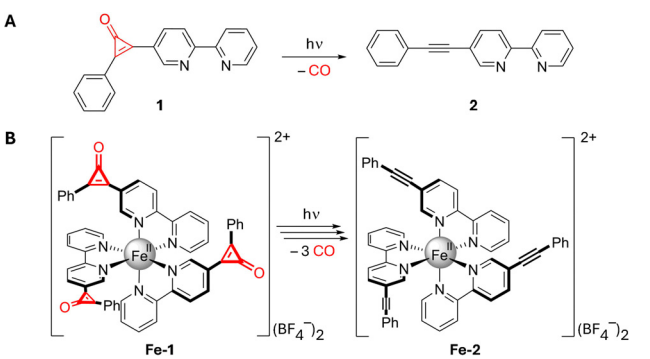

Fig. 1 (A) Reaction scheme for the photodecarbonylation of the cyclopropenone-bipyridine **1** to the respective acetylene **2**. (B) Corresponding reaction scheme for the Fe^{II}-CPOne complex **Fe-1** to its Fe^{II}-acetylene product **Fe-2**. For clarity, only the *fac* isomers of the *fac/mer* mixtures for **Fe-1** and **Fe-2** are depicted.

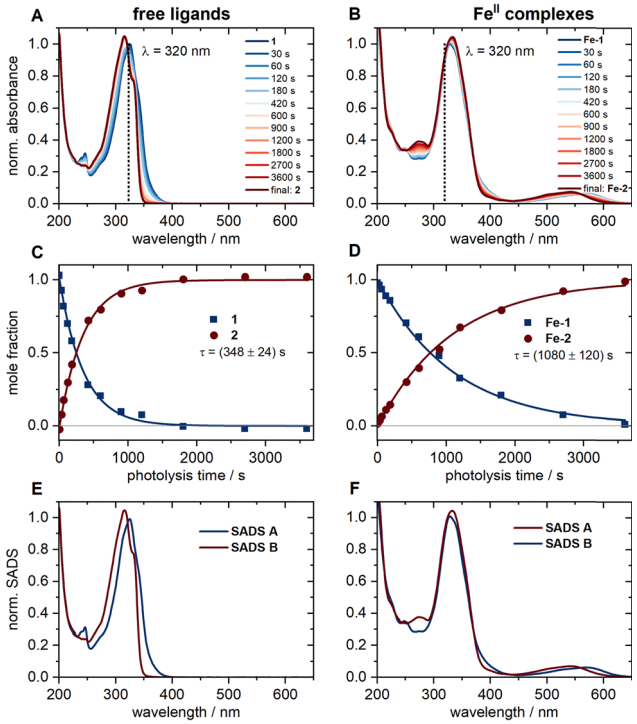

Fig. 2 Normalized UV-vis spectra showing the photolysis *vs.* time of a 360 μM solution of **1** (A) and a 113 μM solution of **Fe-1** (B) upon irradiation with 130 μW of a 320 nm LED. The respective concentration *vs.* irradiation time profiles (C) and (D) and species-associated difference spectra (SADS, (E) and (F)) were obtained by a singular value decomposition (SVD) based analysis of the experimental data. The irradiation conditions were identical for both solutions. The excitation wavelength of 320 nm was chosen as both compounds exhibit an isosbestic point at this wavelength and the overall absorption of the samples thus does not change over time. The intensity transmitted through the samples was further monitored throughout the experiments and remained constant during the measurement. The concentration of **1** was set ∼ 3 times higher than that of **Fe-1** for an equimolar amount of cyclopropenone ligand in both solutions. Still, the decarbonylation of **1** can be seen to proceed much faster than that of **Fe-1**.

cyclopropenone ligand **1** to its acetylene product **2**, and on the evidently much more intricate photodynamics of the corresponding Fe^{II} complex **Fe-1**.[6]

Experimental details

Materials

The syntheses of compounds **1**,[6] **2**,[6] **Fe-1**[6] and **Fe-2**[6] are described in detail in Section S4 of the ESI.†

Steady-state spectroscopy

Unless indicated otherwise, all stationary UV-vis spectra were recorded in spectroscopic grade acetonitrile (Uvasol®) on a Shimadzu UV-2410 desktop spectrometer in a 1 cm (for concentrations of 20 μM or less) or 1 mm quartz cuvette under air. For the stationary photodecarbonylation experiment, the absolute irradiation intensities of the high-power LED were determined behind the cuvettes with a calibrated power meter (Coherent PS19Q). As both irradiation experiments were conducted under identical conditions—including irradiation wavelength, geometry, intensity, and sample volume—and given that the chosen wavelength corresponds to an isosbestic point, the data allows for a meaningful comparison of the quantum yields for decarbonylation of both compounds.

Femtosecond time-resolved electronic absorption spectroscopy (fs-TEAS)

The setup used for femtosecond time-resolved electronic absorption spectroscopy (fs-TEAS) has been described in some detail elsewhere.[7–10] Briefly, it consists of a Ti:Sa regenerative amplifier (Clark MXR CPA 2001) delivering pulses of 120 fs FWHM (full width at half maximum) at 1 kHz repetition rate at a center wavelength of λ = 775 nm. The main part of the 775 nm beamline is used to run a home-built non-collinear optical parametric amplifier (NOPA) with a subsequent prism pulse compressor. Excitation pulses at 600 nm were provided directly by the compressed NOPA. Excitation pulses in the UV at 340 nm were obtained by sum-frequency generation (SFG) between the 600 nm NOPA output and the 775 nm laser fundamental in a type I BBO crystal. For broadband detection, a small fraction of the laser fundamental is sent through a CaF_2 plate to generate supercontinuum probe pulses in the range 325 nm $< \lambda_{probe} <$ 750 nm. These are split into probe and reference beams, dispersed in a prism spectrograph and detected using fast frame-transfer CCD cameras. The pump and probe beams overlap in our sample flow cell of 1 mm optical pathlength which is connected to a reservoir with 100 ml volume. The focal size of the pump beams was ∼ 300 μm and the size of the probe beam at the same spot is ∼ 150 μm. The pump polarization was set to magic angle with respect to the probe polarization in all measurements. An optical chopper in the probe beam path, operated at half the repetition rate, blocks every second probe pulse, while another chopper in the pump beam path, operated at a quarter of the repetition rate, allows two consecutive pump pulses to pass while blocking the next two. In this way, it is possible to record transient absorption difference spectra background-corrected for scattered pump light. The sample was continuously recycled during the measurements and UV-vis spectra were taken before and after each measurement to ensure the integrity of the sample. These spectra are displayed in Fig. S4 (ESI†). To study the dynamics following ligand excitation 80 μM solutions of **1** and **2** as well as 58 μM solutions of **Fe-1** and **Fe-2** in acetonitrile were excited at λ_{pump} = 340 nm at fluence of 0.63 mJ cm^{-2}, respectively. To study the dynamics following excitation of the MLCT bands 115 μM solutions of **Fe-1** and **Fe-2** were excited at λ_{pump} = 600 nm at a fluence of 1.41 mJ cm^{-2}.

Results and discussion

Steady-state spectroscopy

The UV-vis absorption spectra of the compounds are depicted in Fig. 2A and B. The respective spectra in units of molar extinction can be found in Fig. S2 in the ESI.† As can be seen,

the two ligand spectra appear quite similar at first glance, owing to the related π-electron systems, but differ when it comes to some of their finer structures. The same applies to the two Fe^{II} complexes. The observed features were analysed by time-dependent density functional (TD-DFT) calculations[11] to explore the nature of the first 20 (**1** and **2**) and 40 (**Fe-1** and **Fe-2**) excited singlet states, respectively (Section S1, ESI†). Fig. S1 (ESI†) depicts the computed electronic transitions and spectra. Both **1** and **2** show the expected strong ππ* bands in the UV region at nearly identical wavelengths. For **1**, the nπ* transition associated with the free electron pair of the carbonyl oxygen leads to an additional weak shoulder towards longer wavelengths.[3,12] **Fe-1** and **Fe-2** feature additional absorption bands in the vis region between ~500 and 600 nm, and their intense UV bands appear slightly broadened. The TD-DFT calculations for both complexes predict a multitude of transitions in the respective wavelength ranges. The character of the vertical singlet transitions was derived by analysis of the transition density matrices[13] (Fig. S1, ESI†). We conclude that the observed vis absorption band is governed by metal-to-ligand charge transfer (MLCT) transitions. The main UV absorption band still originates from a local ππ* transition within one ligand (ligand-centred, LC) and from ππ* transitions between ligands (ligand-to-ligand charge transfer, LLCT). The presence of some less intense MLCT and metal-centred (MC) transitions is noted as well.

Photodecarbonylation of **1** to **2**, and **Fe-1** to **Fe-2**, respectively, was followed by UV-vis spectroscopy upon irradiation in the UV with a 320 nm light-emitting diode (LED). Fig. 2C and D show the spectral evolution and concentration profiles of the reactants and products during the photolysis and were obtained from a singular value decomposition (SVD) analysis applying a sequential kinetic model of type $A \xrightarrow{\tau} B$. Note that the photodecarbonylation of **Fe-1** to **Fe-2** is a multistep process involving intermediate species with only one or two ligands in the acetylene form. The recorded UV-vis spectra show isosbestic points at all times, so that the assumption of such a model seems justified. Consequently, the obtained species-associated difference spectra (SADS) displayed in Fig. 2E and F reproduce the experimental absorption spectra. The results demonstrate that the photodecarbonylation process in **Fe-1** is slower by about a factor of 3, indicating that the presence of the Fe^{II} ion leads to a decrease in the quantum yield of photodecarbonylation by a factor of about 10 (see ESI,† Section S2) compared to **1**. Furthermore, irradiation of the MLCT band of **Fe-1** in the vis spectral range does not cause any noticeable decarbonylation (Fig. S3, ESI†).

Femtosecond time-resolved electronic absorption spectroscopy (fs-TEAS)

The measured femtosecond time-resolved electronic absorption maps uncovered the ultrafast photochemical dynamics of **1** and **Fe-1** (Fig. 3). The experimental data were recorded after excitation of **1** and **Fe-1** at λ_{pump} = 340 nm (Fig. 3A and B, respectively) and excitation of **Fe-1** at λ_{pump} = 600 nm (Fig. 3C).

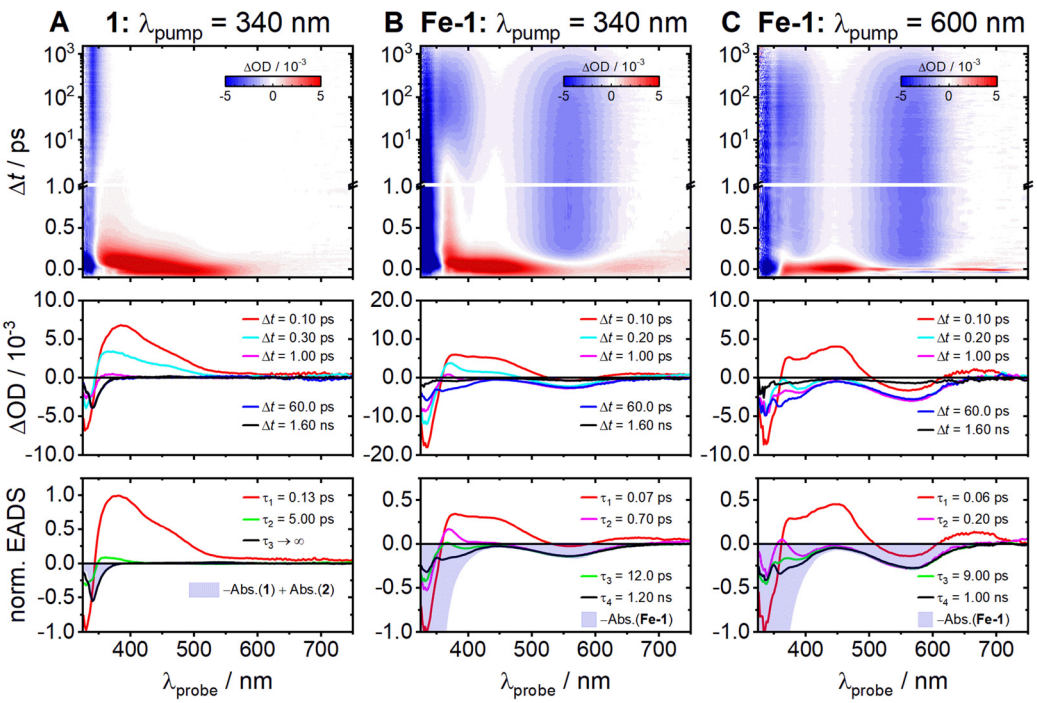

Fig. 3 Two-dimensional time-resolved electronic absorption maps recorded in acetonitrile (top), transient absorption difference spectra at selected decay times (middle) and EADS with global time constants used for the modeling of the experimental spectra (bottom) for **1** and **Fe-1** (columns A and B, respectively) after photoexcitation at λ_{pump} = 340 nm and for **Fe-1** (C) after excitation at λ_{pump} = 600 nm. The data for **1** were corrected for contributions from the acetylene product **2** as described in the ESI.†

Auxiliary measurements on the photodynamics of the acetylene ligand **2** and its complex **Fe-2** are given in the ESI† (Fig. S6 and S9). Since the photodecarbonylation of cyclopropenone **1** is highly efficient, subsequent photoexcitation of the resulting acetylene product **2** is in practice unavoidable due to some accumulation in the sample reservoir, leading to artifacts in the recorded transient absorption map for **1**. Consequently, the raw TEAS data for **1** (Fig. S6A, ESI†) were corrected for the contribution of the excited acetylene product to the transient absorption signal (see ESI,† Section S3 and Fig. S6 for a description of the correction procedure) and Fig. 3A depicts the corrected transient absorption results.

The fs-TEAS results for the free cyclopropenone **1** reveal an initially broad excited-state absorption (ESA) that decays very rapidly in <1 ps, accompanied by a substantial blue-shift (Fig. 3A). The intense ground-state bleach (GSB) at λ_{probe} < 350 nm, which appears immediately after photoexcitation, remains for the entire 1.6 ns experimental observation time. These data were successfully modelled using the python-based software package KiMoPack[14] assuming a consecutive kinetic model. The resulting evolution-associated difference spectra (EADS) with their associated global time constants are given in the bottom row of Fig. 3. As can be seen, three spectral components were sufficient to describe the dynamics. The first EADS associated with time constant τ_1 = 0.13 ± 0.02 ps describes the rapid decay of the broad initial ESA signal. The second decays with τ_2 = 5.0 ± 3.0 ps and exhibits a similar shape but much smaller amplitude. The final component ($\tau_3 \rightarrow \infty$) is negative in the region of the GSB and does not show any recognizable decay. Since it matches the scaled ground-state absorption difference spectrum –Abs(**1**) + Abs(**2**) (blue-shaded area in Fig. 3A bottom), it can be reasonably attributed to the formation of the acetylene photoproduct **2** from **1**.

Turning to the cyclopropenone **Fe-1** complex, the obtained fs-TEAS maps in Fig. 3B and C reveal very different pictures compared to free **1**. At the two excitation wavelengths of 340 and 600 nm, however, the maps for **Fe-1** appear rather similar. The observed broad, intense, initial ESA band from ~370 to 540 nm undergoes a swift transformation into a distinct narrow peak at λ_{probe} = 370 nm, which stands out especially after excitation in the UV (Fig. 3B). Shortly thereafter, the ESA transforms into negative GSB contributions, followed eventually by gradual, yet largely full recoveries towards the end of the observation time window ($\Delta t \sim$ 1.6 ns). The global analyses gave similar EADS and time constants at both excitation wavelengths. The first component describes the decay of the broad initial ESA and establishment at λ_{probe} < 350 nm of the GSB. The associated time constant τ_1 = 70 ± 15 fs (60 ± 25 fs for λ_{pump} = 600 nm) reflects dynamics occurring on time scales close to or even below our experimental time resolution, which in both measurements was of the order of $\Delta t \sim$ 50 fs. The following two EADS mainly show the loss of the spectral signatures at λ_{probe} = 370 nm with τ_2 = 0.7 ± 0.3 ps (0.2 ± 0.1 ps for λ_{pump} = 600 nm) and τ_3 = 12.0 ± 5.0 ps (9.0 ± 6.0 ps). The final EADS carries mainly GSB contributions from the MLCT-related absorption features, as evidenced by the scaled negative ground state absorption spectrum (–Abs.(**Fe-1**), blue-shaded area). The associated time constants of τ_4 = 1.2 ± 0.1 ns (1.0 ± 0.2 ns) describe the largely complete recovery of the initial ground state population. As can be seen from the last transient spectra, plotted at Δt = 1.6 ns after excitation (black lines in Fig. 3B and C), we observe little to virtually no final reaction product formation under the femtosecond experimental conditions at both excitation wavelengths, even after excitation at λ_{pump} = 340 nm. This is in strong contrast with the results for free **1** (Fig. 3A), and with the observed slow photodecarbonylation of **Fe-1** to **Fe-2** in the static photolysis experiment (*cf.* Fig. 2). We speculate—although this assertion requires further investigation—that the photodecarbonylation

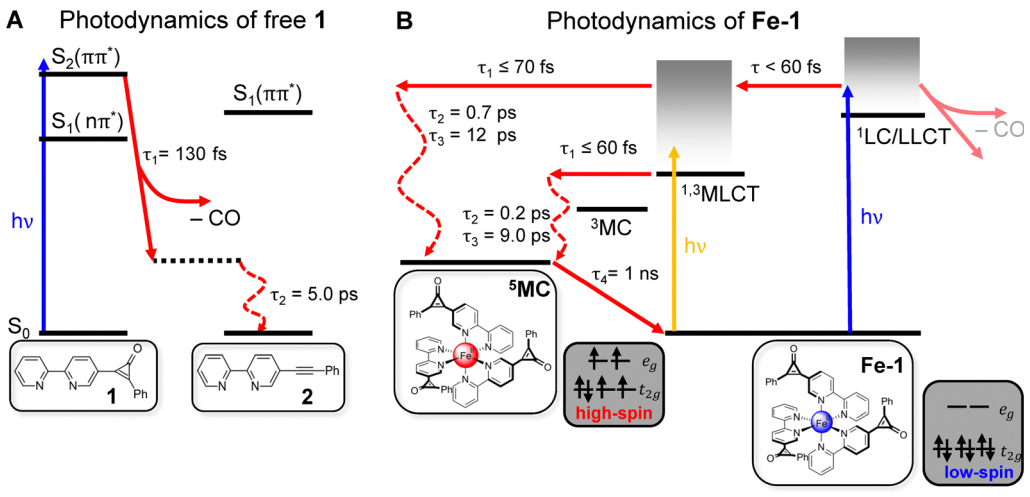

Fig. 4 Proposed relaxation scenarios derived from the fs-TEAS results for the free cyclopropenone ligand **1** and its complex **Fe-1**. (A) Excitation of **1** leads to ultrafast CO release forming the acetylene product **2** in ~ 130 fs. (B) Excitation of a ligand-centred (LC) excited state of **Fe-1** is followed by ultrafast energy transfer *via* intermediate singlet and triplet metal-to-ligand charge transfer (^{1,3}MLCT) and triplet metal-centred (^{3}MC) states to the high-spin quintet MC state (^{5}MC). The same state is also formed upon excitation of **Fe-1** in the ^{1}MLCT band with visible light. This competing ultrafast spin crossover (SCO) process supresses the release of CO from **Fe-1**.

of **Fe-1** in the static UV experiment may be due to partial dissociation and photolysis of the unbound ligand **1** in equilibrium. Experimental evidence for the presence of such an equilibrium can be found in the UV-vis spectra of **Fe-1** at different concentrations (*cf.* Fig. S5, ESI†). Interestingly, the ultrafast dynamics of the cyclopropenone complex **Fe-1** (Fig. 3B) and the acetylene complex **Fe-2** (Fig. S9, ESI†) appear very similar.

The above results can be rationalized based on the relaxation schemes in Fig. 4A and B. According to Fig. 4A, initial excitation at λ_{pump} = 340 nm populates the lowest-lying $^1\pi\pi^*$ state of cyclopropenone **1**. In previous studies of related cyclopropenones, a rapid sub-200 fs decay of an initial ESA signal was assigned to the loss of CO from the photoproduced $^1\pi\pi^*$ state and the formation of the acetylene either in the excited or in the ground state.[3–5] In our case, therefore, we link the 130 fs time constant τ_1 to this decarbonylation process giving **2** in its electronic ground state. We assign the second time constant τ_2 = 5.0 ps to subsequent structural dynamics in the ground state of **2** from an assumed "*cis*-bent" intermediate.[3] The formation of **2** was clearly identified from the persistent final TEA spectrum in Fig. 3A that matches the (negative) ground state absorption difference spectrum of **1** and **2**. The ultrashort 130 fs time constant characterizing the CO elimination thus accounts for the observed remarkable decarbonylation efficiency of **1**, as reported for other cyclopropenones,[15] with a quantum yield likely close to unity.

This picture completely changes in the case of **Fe-1** where cyclopropenone **1** is bound to the Fe^{II} centre as a ligand (Fig. 4B). In fact, the photodynamics of **Fe-1** has to be discussed in the context of other Fe^{II} polypyridyl complexes such as the well-studied, structurally related $[Fe(bpy)_3]^{2+}$. Investigations of this[16–24] and related[25–30] complexes demonstrated that photoexcitation of the ^{1}MLCT band in the vis spectrum results in the formation of an excited metal-centred (MC) state, in which the Fe^{II} centre ion adopts quintet spin multiplicity (^{5}MC) and is thus in the Fe^{II} high-spin state. The ensuing spin crossover (SCO) after ^{1}MLCT excitation has been found to occur extraordinarily fast, in $<$ 50 fs, resulting in a quantum yield close to unity.[31] This indicates that potential intermediates, such as ^{3}MLCT and ^{1,3}MC states, are traversed on even shorter time scales.[21] Recent two-dimensional femtosecond spectroscopic measurements actually suggested parallel relaxation pathways *via* the ^{3}MLCT state and directly to the MC states.[23] In either case, these literature results suggest a blue-print regarding our observations for **Fe-1** after MLCT excitation at λ_{pump} = 600 nm. The very broad observed initial ESA is a typical signature of the MLCT states.[18,21,25] The rapid decay time of τ_1 = 60 fs close to the instrument response function (IRF) of our experiment should in fact be viewed as upper limit for this process (*i.e.*, $\tau_1 \leq$ 60 fs). The subsequent appearance of the mostly negative transient absorptions governed by the GSB of the MLCT states (*cf.* Fig. 3B) indicates the population of the ^{5}MC state. This state is formed with some excess energy and undergoes vibrational relaxation with τ_2 = 0.2 ps and τ_3 = 9 ps as intermediate time constants.[26,27] The reverse intersystem crossing leading to the recovery of the singlet ground state (^{1}GS) eventually occurs within the typical ^{5}MC lifetime of $\tau_4 \sim$ 1 ns in acetonitrile.[28]

Remarkably, similar dynamic processes are also seen for **Fe-1** upon excitation at λ_{pump} = 340 nm, where the initial absorption of the ^{1}GS is governed by the ^{1}LC/LLCT bands of the ligands. However, the initially observed transient state that decays within near response-limited $\leq$ 60 fs is already associated with the MLCT states, suggesting that the ^{1}LC/LLCT to MLCT transition is already virtually complete within the time resolution of our experiment. A similarly efficient funnelling of UV excitation in MC excited states has been implicitly observed in $[Fe(bpy)_3]^{2+}$ before.[22] The intermediate time constants τ_2 = 0.7 ps and τ_3 = 12 ps can again be assigned to relaxation dynamics in the ^{5}MC state. The slight differences in relaxation times between the measurements might be a result of the ^{5}MC state being accessed at different crossing points from the MLCT manifold.[19] Ultimately, full recovery of the ^{1}GS state is observed with $\tau_4 \sim$ 1 ns, leaving little if any indication for release of CO from complex **Fe-1**. Attempts to study CO release in the absence of competing spin crossover using the related high-spin complex **Fe-3** (Section S4, ESI†) were unfortunately not possible due to the formation of multiple metal complexes.

Conclusion

In conclusion, we showed that the irradiation time required for photodecarbonylation of cyclopropenone **1** to acetylene **2** in stationary experiments is significantly increased when the molecule coordinates as a ligand to an Fe^{II} centre ion as in the complex **Fe-1**. As revealed by our fs-TEAS measurements, this is due to an ultrafast SCO to the high-spin form of the **Fe-1** complex in $<$ 60 fs (possibly only $\sim$ 20 fs[23]). This behaviour is observed in many Fe^{II} polypyridyl complexes after excitation of their MLCT bands in the vis spectral range. We further demonstrated that excitation in the UV of the ligand absorption bands of the **Fe-1** complex triggers a similar ultrafast process that outcompetes the expected photochemical CO release.

These results reveal a number of interesting insights into the photodynamics as well as prospective applications of M–CPOnes. Firstly, while previous studies have shown that coordination to d^6 ions can strongly suppress the *trans–cis* photoisomerisation kinetics of azopyridines,[32,33] it remains remarkable that the coordination of cyclopropenone **1** to Fe^{II} within **Fe-1** is sufficient to almost completely eliminate photorelease of CO from this ligand, despite the fact that the latter process happens in only $\sim$ 130 fs in the free ligand **1** itself. Since the photodecarbonylation of **Fe-1** can be achieved through continuous static irradiation—albeit with a significantly lower quantum yield than the free ligand—it remains unclear whether this process also occurs from coordinated ligands with low efficiency or only *via* photoexcitation of transiently de-coordinated ligands in equilibrium. Structure-sensitive ultrafast time-resolved vibrational spectroscopy in the carbonyl region could provide valuable insights, as the ground-state bleach (GSB) signals of the cyclopropenone species are less likely to interfere with potential product absorptions.

Secondly, the Fe^{II} metal centre is appealing for applications since there is the potential to extend the M-CPOne absorption to the *vis* and near-infrared (NIR) regions, outstripping the capabilities of other readily accessible M-CPOnes with first-row transition metals like Zn^{II} and Co^{II} that exhibit MLCT states at considerably higher energies.[6] Moreover, the viability of inducing CO release from an initially excited MLCT state warrants exploration of systems featuring longer MLCT lifetimes. A multitude of strategies aiming at extended MLCT lifetimes in Fe^{II} complexes are already within reach.[34] In addition, the Ru^{II} analogue, with its similar MLCT energy but lack of SCO due to its substantial ligand field splitting, might hold promise for expanding our understanding of the dynamics.[35–38] Another interesting feature is the presence of LLCT states in these systems that may enable excitation of multiple ligands with a single photon, potentially achieving quantum yields greater than one. In this context, the Zn^{II} analogue could be a viable candidate. Due to its closed-shell nature, Zn^{II} acts as an electronic coupling centre for the ligands, while the complex itself is devoid of low-lying MLCT and MC states that could interfere with the photodecarbonylation. Lastly, the intriguing prospect of introducing other chromophores as the second cyclopropenone substituent may open diverse opportunities to control the excitation wavelength for CO release.[6]

Data availability

Data supporting this article have been included in the ESI.†

Conflicts of interest

There are no conflicts to declare.

Acknowledgements

We thank the Deutsche Forschungsgemeinschaft (DFG, project number 413396832) for financial support and the spectroscopy department of the Otto Diels-Institute of Organic Chemistry for NMR and mass spectral data collection.

Notes and references

1 E. W.-G. Diau, J. L. Herek, Z. H. Kim and A. H. Zewail, *Science*, 1998, **279**, 847.
2 M.-H. Kao, R. K. Venkatraman, M. N. R. Ashfold and A. J. Orr-Ewing, *Chem. Sci.*, 2020, **11**, 1991.
3 S. Takeuchi and T. Tahara, *J. Chem. Phys.*, 2004, **120**, 4768.
4 A. Poloukhtine and V. V. Popik, *J. Phys. Chem. A*, 2006, **110**, 1749.
5 S. C. Doan, G. Kuzmanich, M. N. Gard, M. A. Garcia-Garibay and B. J. Schwartz, *J. Phys. Chem. Lett.*, 2012, **3**, 81.
6 M. Lehr, T. Neumann, C. Näther and A. J. McConnell, *Dalton Trans.*, 2022, **51**, 6936.
7 K. Röttger, S. Wang, F. Renth, J. Bahrenburg and F. Temps, *Appl. Phys. B*, 2015, **118**, 185.
8 S. Wang, M. Bohnsack, S. Megow, F. Renth and F. Temps, *Phys. Chem. Chem. Phys.*, 2019, **21**, 2080–2092.
9 F. Renth, M. Foca, A. Petter and F. Temps, *Chem. Phys. Lett.*, 2006, **428**, 62–67.
10 K. Röttger, R. Siewertsen and F. Temps, *Chem. Phys. Lett.*, 2012, **536**, 140–146.
11 C. Adamo and D. Jacquemin, *Chem. Soc. Rev.*, 2013, **42**, 845.
12 Z. Yoshida and H. Miyahara, *Bull. Chem. Soc. Jpn.*, 1972, **45**, 1919.
13 F. Plasser, *J. Chem. Phys.*, 2020, **152**, 084108.
14 C. Müller, T. Pascher, A. Eriksson, P. Chabera and J. Uhlig, *J. Phys. Chem. A*, 2022, **126**, 4087.
15 R. W. Fessenden, P. M. Carton, H. Shimamori and J. C. Scalano, *J. Phys. Chem.*, 1982, **86**, 3803.
16 J. K. McCusker, K. N. Walda, R. C. Dunn, J. D. Simon, D. Magde and D. N. Hendrickson, *J. Am. Chem. Soc.*, 1993, **115**, 298.
17 J. K. McCusker, A. L. Rheingold and D. N. Hendrickson, *Inorg. Chem.*, 1996, **35**, 2100.
18 W. Gawelda, A. Cannizzo, V.-T. Pham, F. van Mourik, C. Bressler and M. Chergui, *J. Am. Chem. Soc.*, 2007, **129**, 8199.
19 C. De Graaf and C. Sousa, *Chem. – Eur. J.*, 2010, **16**, 4550.
20 M. Chergui, *Acc. Chem. Res.*, 2015, **48**, 801.
21 G. Auböck and M. Chergui, *Nat. Chem.*, 2015, **7**, 629.
22 M. Fondell, S. Eckert, R. M. Jay, C. Weniger, W. Quevedo, J. Niskanen, B. Kennedy, F. Sorgenfrei, D. Schick, E. Giangrisostomi, R. Ovsyannikov, K. Adamczyk, N. Huse, P. Wernet, R. Mitzner and A. Föhlisch, *Struct. Dyn.*, 2017, **4**, 054902.
23 A. Lee, M. Son, M. Deegbey, M. D. Woodhouse, S. M. Hart, H. F. Beissel, P. T. Cesana, E. Jakubikova, J. K. McCusker and G. S. Schlau-Cohen, *Chem. Sci.*, 2023, **14**, 13140.
24 C. Zahn, M. Pastore, J. L. P. Lustres, P. C. Gros, S. Haacke and K. Heyne, *J. Am. Chem. Soc.*, 2024, **146**, 9347.
25 J. E. Monat and J. K. McCusker, *J. Am. Chem. Soc.*, 2000, **122**, 4092.
26 C. Brady, P. L. Callaghan, Z. Ciunik, C. G. Coates, A. Døssing, A. Hazell, J. J. McGarvey, S. Schenker, H. Toftlund, A. X. Trautwein, H. Winkler and J. A. Wolny, *Inorg. Chem.*, 2004, **43**, 4289.
27 A. L. Smeigh, M. Creelman, R. A. Mathies and J. K. McCusker, *J. Am. Chem. Soc.*, 2008, **130**, 14105.
28 J. Tribollet, G. Galle, G. Jonusauskas, D. Deldicque, M. Tondusson, J. F. Letard and E. Freysz, *Chem. Phys. Lett.*, 2011, **513**, 42.
29 N. Huse, H. Cho, K. Hong, L. Jamula, F. M. F. De Groot, T. K. Kim, J. K. McCusker and R. W. Schoenlein, *J. Phys. Chem. Lett.*, 2011, **2**, 880.
30 C. Sousa, C. De Graaf, A. Rudavskyi and R. Broer, *J. Phys. Chem. A*, 2017, **121**, 9720.
31 M. A. Bergkamp, C. K. Chang and T. L. Netzel, *J. Phys. Chem.*, 1983, **87**, 4441.
32 S. Megow, H. L. Fitschen, F. Tuczek and F. Temps, *J. Phys. Chem. Lett.*, 2019, **10**, 6048.
33 K. Yamaguchi, S. Kume, K. Namiki, M. Murata, N. Tamai and H. Nishihara, *Inorg. Chem.*, 2005, **44**, 9056.
34 O. S. Wenger, *Chem. – Eur. J.*, 2019, **25**, 6043.

35 A. Juris, V. Balzani, F. Barigelletti, S. Campagna, P. Belser and A. von Zelewsky, *Coord. Chem. Rev.*, 1988, **84**, 85.
36 N. H. Damrauer, G. Cerullo, A. Yeh, T. R. Boussie, C. V. Shank and J. K. McCusker, *Science*, 1997, **275**, 54.
37 A. N. Tarnovsky, W. Gawelda, M. Johnson, C. Bressler and M. Chergui, *J. Phys. Chem. B*, 2006, **110**, 26497.
38 A. Cannizzo, F. van Mourik, W. Gawelda, G. Zgrablic, C. Bressler and M. Chergui, *Angew. Chem., Int. Ed.*, 2006, **45**, 3174.

